Rate equations for the control of Yb-171 ions

A. E. Iyer[1], **C. M. Steenkamp**[1,2] **and N. E. Payne**[1]

[1]Stellenbosch Photonics Institute, Physics Department, Stellenbosch University, Stellenbosch, 7600, South Africa
[2]National Institute for Theoretical and Computation Sciences, South Africa

E-mail: 23171480@sun.ac.za

Abstract. Rate equations are used to calculate the hyperfine state population dynamics of an ensemble of ytterbium-171 ions in interaction with lasers. The application is to optimize the efficiency and timescales of quantum control processes that we plan to use in the lab. The effect of laser powers, polarisations and side-band carrier ratios for Doppler cooling and state preparing are investigated.

1 Introduction

Trapped ions are a leading physical implementation of qubits which can be used in quantum computers offering long coherence times, scalability and the ability to be precisely controlled using lasers [1]. This study is part of a quantum control project with the long term aim to realise unsharp measurements between two weakly entangled ytterbium ion isotopes, $^{171}\mathrm{Yb}^{+}$ and $^{174}\mathrm{Yb}^{+}$, in a linear Paul trap [2].

The basic control processes that must be achieved in the laboratory are Doppler cooling, state preparation, state detection and electron shelving. Doppler cooled reduces the temperature of the ions by cycles of absorption of red-detuned laser photons and spontaneous emission. During state preparation the ion is optically pumped into the qubit ground state. Electron shelving is achieved by populating and depopulating a long-lived metastable state. State detection is achieved by pumping a closed-loop transition that produces measurable fluorescence. Additional repump lasers are required to recover ions that have spontaneously decayed into dark states during the control processes.

The Einstein rate equations are a set of coupled first-order differential equations describing the time-dependent evolution of the ion's hyperfine state populations. Rate equations are suitable to describe atom-laser interactions, where the decay of the coherence between quantum levels is faster than the timescales on which we manipulate them, as is the case in our system. [3]. We use a rate equation model to calculate the hyperfine state population of $^{171}\mathrm{Yb}^{+}$ during the quantum control processes that would be used in the experiment, to gain insights on how to increase the efficiency and estimate timescales. The numerical model includes up to 60 atomic states and 11 experimental parameters. The model is used to inform parameter choices in the laboratory and understand the timescales observed in the experiments.

2 Einstein rate equations

The interaction between an atom with states $|i\rangle$ and $|j\rangle$ and light that is close to resonance with the energy spacing between these states is described using the Einstein coefficients A and B. Specifically, the term A_{ij} (in s^{-1}) describes the spontaneous emission from a non-degenerate hyperfine state i to another single non-degenerate hyperfine state j. The term B_{ji} describes stimulated emission and B_{ij} stimulated absorption (both in $J^{-1}\cdot m^{3}\cdot s^{-2}$).

Using the Wigner-Eckhart theorem [3, 4], A_{ij} can be written as

$$A_{ij} = A_{J'J}(2J'+1)(2F'+1)\begin{Bmatrix} J & J' & k \\ F' & F & I \end{Bmatrix}^{2} \left\langle Fm_F \middle| F'm'_{F'}kq \right\rangle^{2}, \tag{1}$$

where dashes denote state $|i\rangle$. The value k is the rank of the tensor operator involved, i.e. the rank of the electric dipole operator is 1 and the rank of the electric quadrupole operator is 2. The quantum numbers in the expression are F for the total angular momentum, m_F for the magnetic quantum, J for the total electronic angular momentum, I for the nuclear spin, and q can be interpreted as the projection of the photon angular momentum onto the quantisation axis. $A_{J'J}$ is the total spontaneous decay rate from the excited term to the ground term. This expression includes the Wigner-6j symbol and Clebsch-Gordon coefficient to calculate the transition rates for each pair of hyperfine states for different light polarizations.

The Einstein coefficient B_{ij} is calculated using the relation between the Einstein coefficients, $A_{ij} = \frac{\hbar\omega^3_{J'J}}{\pi^2 c^3} B_{ij}$. We treat each atomic state individually, so that the degeneracy is 1 for all states, hence $B_{ij} = B_{ji}$.
The generalized expression for a rate equation is,

$$\frac{dn_i}{dt} = \sum_{j=1, j\neq i}^{j=N} (n_j B_{ji} P(\omega) + n_j A_{ji} - n_i B_{ij} P(\omega) - n_i A_{ij}), \tag{2}$$

where N is the number of states in the model, n_i represents the probability of finding the system in state $|i\rangle$. The term $P(\omega)$ is the total energy density $P(\omega) = \int_0^\infty \rho(\omega) s(\omega) d\omega$ in $J \cdot m^{-3} \cdot s$. The atomic line-shape is described using a gaussian function $s(\omega)$, centered around the atomic resonance frequency [3]. The laser spectral distribution $\rho(\omega)$ is also modeled as a gaussian function of angular frequency ω and of laser properties such as laser intensity, bandwidth and detuning.
We express the set of rate equations in equation 2 in matrix form $\frac{d}{dt}\vec{n} = (M^{\text{spont}} + M^{\text{stim}})\vec{n}$ and solve them numerically in MATLAB using the ClebschGordan.m [5], Wigner6j.m [6] and Wigner3j.m [7] functions.

3 Results and discussion

The relevant 20 atomic states of $^{171}\text{Yb}^+$ are shown in Figure 1. The ground and excited qubit states in the $^2\text{S}1/2$ manifold are labeled $|0\rangle$ and $|1\rangle$. The laser-driven transitions included in the model are numbered, with the wavelength and sideband frequency indicated in the legend. The results of the rate equation model for a given set of laser parameters is the population evolution of the 60 hyperfine states for a specified time.

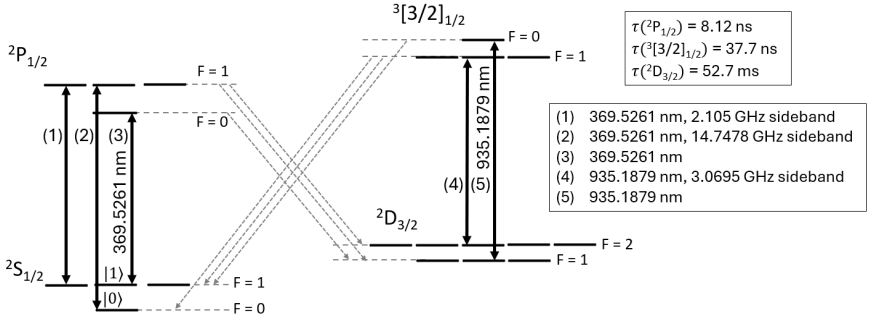

Figure 1: $^{171}Yb^+$ level scheme with laser-pumped transitions (solid) and relevant decays (dashed). The wavelengths and sideband frequencies are indicated in the top left corner legend. The spontaneous decay rates for each level are captured in the top right corner legend.

To achieve Doppler cooling transitions (3) and (2) are pumped by the 369 nm laser with a 14.7 GHz first order upper sideband respectively to the $^2P_{1/2}$ states (lifetime 8.12 ns) [8]. In the experiment the 369 nm laser is red detuned by approximately 200 MHz so that it interacts most strongly (resonantly) with ions moving anti-parallel to the direction of propagation of the laser. In the simulation on-resonance 369 nm light is used during Doppler cooling to simulate these moving atoms interacting with resonant light due to the Doppler shift. Cooling takes place when the ion undergoes sequential $^2S_{1/2} -^2 P_{1/2}$ absorption-spontaneous emission cycles, that reduce the ion's momentum parallel to the laser beam. During cooling, a branching ratio of 0.5% from $^2P_{1/2}$ to the long-lived $^2D_{3/2}$ states (lifetime of 52.7 ms) removes ions from the cooling cycle. Figure 2 shows the the importance of the repump laser during Doppler cooling. In the absence of the repump laser, population accumulates in the $^2D_{3/2}$ states to a fraction of approximately 0.16 within 5 ps, whereas repumping maintains the $^2D_{3/2}$ below a fraction of 0.01. This is important as ions in the $^2D_{3/2}$ states do not participate in cooling, making the cooling inefficient.

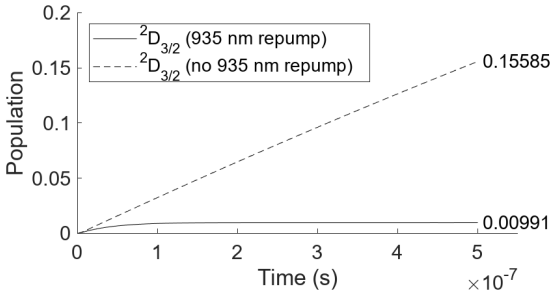

Figure 2: Accumulation of population in the $^2D_{3/2}$ states during Doppler cooling with and without 935 nm repumping. The 369 nm cooling laser power was implemented using sideband and carrier power percentages at 5% and 88.6%, respectively, of the total unmodulated carrier power, $48.4\mu W$. The sideband percentage corresponds to the 14.7 GHz sideband used during Doppler cooling. The 935 nm laser used sideband and carrier power percentages at 5.6% and 83.28%, respectively, of the total unmodulated carrier power, 0.49 mW. Both laser use equal vertical and horizontal components.

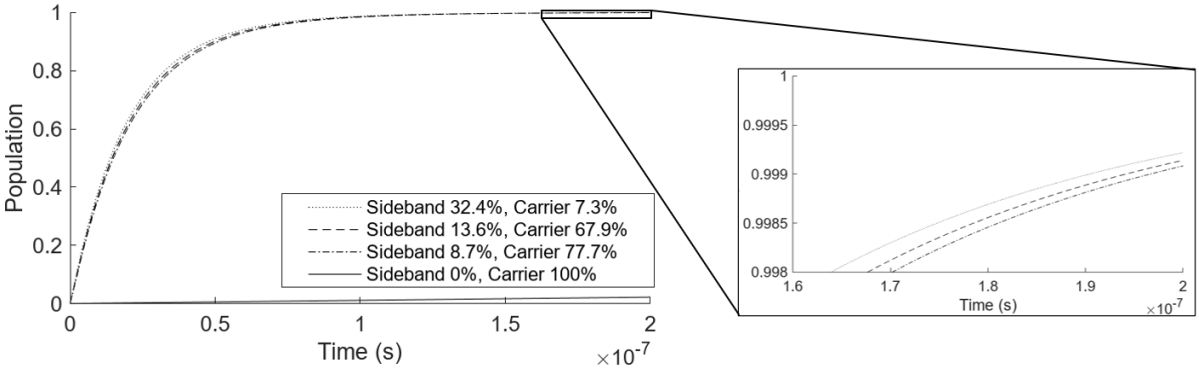

Figure 3: (Left) Increase in the $|0\rangle$ state population during state preparation for different 369 nm laser sideband-carrier ratios as measured in the laboratory and expressed as percentages of the total unmodulated carrier power, $48.4\mu W$. The initial state used for all runs is the final state after Doppler cooling ions from a pure excited state $|1\rangle$ for 50 ns. The 935 nm laser conditions were kept constant using both vertical and horizontal polarisation; and sideband and carrier power percentages at 5.6% and 83.28%, respectively, of the total unmodulated carrier power, 0.49 mW. (Right) Enlarged section of graph.

Qubits are initialized by pumping into the $|0\rangle$ state using the 369 nm laser and a 2.1 GHz first order upper sideband driving transitions (3) and (1) respectively (Figure1). Figures 3 and 4 show the population in the $|0\rangle$ state as measure of the efficiency of state preparation under different laser parameters. Figure 3 shows that the 2.1 GHz sideband is essential to enable optical pumping into the $|0\rangle$ state. As sideband modulation increases, second order sidebands increase in size — decreasing the power distributed between the first order sideband used for our processes and the carrier beam. Figure 4 shows that the efficiency of state preparation depends on the laser polarization, with mixed polarisation (equal vertical and horizontal polarization) giving the highest population after 0.2 μs. These results give an indication of the time needed for state preparation under ideal conditions that inform the planning of experimental measurements.
The model was also used to confirm that the populations of the relevant states do not change during state detection by driving transition (3) only.

4 Conclusions

The rate equation model makes it possible to understand the dynamics and time scales in relation to the experimental parameters, such as laser powers and side band powers. The results are useful to inform decisions on experimental parameters in our laboratory. Contradictory to what we expect, the differences between plots in both figure 3 and 4 appear negligible. This is because our energy density quantity is large in all cases and partially

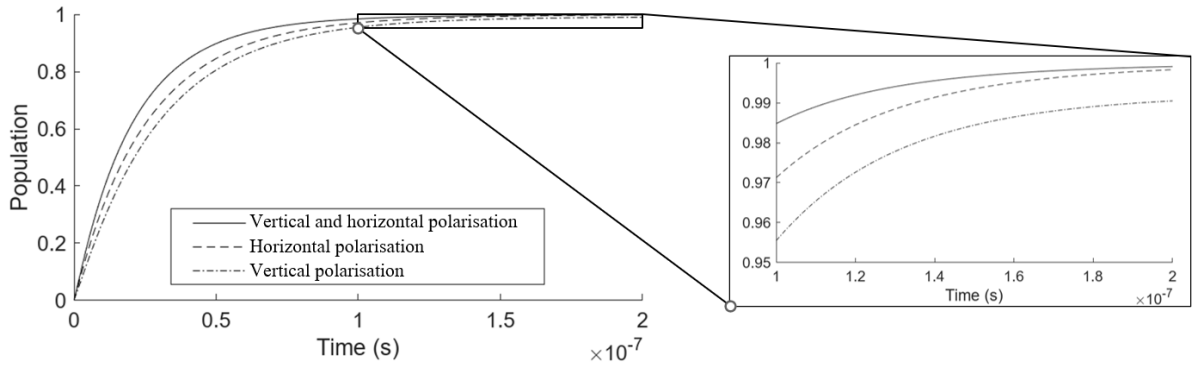

Figure 4: (Left) Increase in the $|0\rangle$ state population during state preparation for different 369 nm and 935 nm laser polarisations in the presence of a vertical magnetic field. The sideband-carrier percentages of the total power for the 369 nm laser were 13.6% and 67.9% respectively and the laser power at 48.4μW. The sideband percentage corresponds to the 2.1 GHz sideband used during state preparation. The sideband-carrier percentages of the total power for the 935 nm laser were 5.6% and 83.28% respectively and the laser power at 0.49 mW. (Right) Enlarged section of graph.

saturates the transition. When reduced, changes in sideband power appear more noticeable. However, overall the results have shown the importance of efficient 935 nm repumping, and that state preparation efficiency is positively affected by the 2.1 GHz modulation and is marginally faster with a combination of both vertical and horizontal polarisation. We are also able to gauge how long state preparation takes under ideal circumstances. A current limitation of the model is that Zeeman shifts due to the external magnetic field has not been implemented yet. Future work includes modeling of a 411 transition from ${}^2S_{1/2}{}^{-2}$ to ${}^2D_{5/2}$, which is a quadrupole transition into a metastable state, using the Optical Bloch Equations [9].

References

[1] H. Häffner, C. Roos, and R. Blatt, "Quantum computing with trapped ions," *Physics reports*, vol. 469, no. 4, pp. 155–203, 2008.

[2] S. Choudhary, T. Konrad, and H. Uys, "Implementation schemes for unsharp measurements with trapped ions," *Phys. Rev. A*, vol. 87, no. 1, p. 012131, 2013.

[3] D. A. Steck, "Quantum and atom optics," 2006, available online at http://steck.us/teaching.

[4] G. K. Woodgate, *ELEMENTARY ATOMIC STRUCTURE.* 1970, 01 1970. [Online]. Available: https://www.osti.gov/biblio/4055778

[5] D. Terr, "Clebschgordan.m," 2025, MATLAB Central File Exchange. Retrieved May 22, 2024. [Online]. Available: https://www.mathworks.com/matlabcentral/fileexchange/5276-clebschgordan-m

[6] A. B. Deb, "Wigner6j.m," 2025, MATLAB Central File Exchange. Retrieved May 22, 2024. [Online]. Available: https://www.mathworks.com/matlabcentral/fileexchange/16187-wigner6j-m

[7] D. Terr, "Wigner3j.m," 2025, MATLAB Central File Exchange. Retrieved May 22, 2024. [Online]. Available: https://www.mathworks.com/matlabcentral/fileexchange/5275-wigner3j-m

[8] J. Eschner, G. Morigi, F. Schmidt-Kaler, and R. Blatt, "Laser cooling of trapped ions," *Journal of the Optical Society of America B*, vol. 20, no. 5, pp. 1003–1015, 2003.

[9] S. Bester and C. Steenkamp, "Optical bloch modeling of magnetic dipole transitions in a four-state system and its application in ion trapping: tutorial," *Journal of the Optical Society of America B*, vol. 40, no. 4, pp. 830–848, 2023.